Local density of states effects at the metal–molecule interfaces in a molecular device

HANS-GERD BOYEN[1]*, PAUL ZIEMANN[1], ULF WIEDWALD[1], VALENTINA IVANOVA[2], DIETER M. KOLB[2], SUNG SAKONG[3], AXEL GROSS[3], ANDRIY ROMANYUK[4], MICHAEL BÜTTNER[4] AND PETER OELHAFEN[4]

[1]Abteilung Festkörperphysik, Universität Ulm, D-89069 Ulm, Germany
[2]Abteilung Elektrochemie, Universität Ulm, D-89069 Ulm, Germany
[3]Abteilung Theoretische Chemie, Universität Ulm, D-89069 Ulm, Germany
[4]Institut für Physik, Universität Basel, Klingelbergstr. 82, CH-4056 Basel, Switzerland
*e-mail: hans-gerd.boyen@uni-ulm.de

Published online: 2 April 2006; doi:10.1038/nmat1607

Clarifying the nature of interactions between metal electrodes and organic molecules still represent one of the challenging problems in molecular electronics that needs to be solved in order to optimize electron transport through a molecular device. For this purpose, electronic properties at metal–molecule interfaces were studied by combining experimental and theoretical methods. Applying a novel electrochemical approach, strictly two-dimensional Pd islands were prepared on top of 4-mercaptopyridine self-assembled monolayers (4MP-SAMs) which, in turn, were deposited on (111)-oriented Au single crystals. Electron spectroscopy together with density functional theory calculations revealed strong interactions between the molecules and the islands due to Pd–N bonds, resulting in a drastically reduced density of states (DOS) at the Fermi level E_F for a nearly closed Pd monolayer, and even non-metallic properties for nanometre-sized islands. Similarly, a significantly reduced DOS at E_F was observed for the topmost Au layer at the Au–SAM interface due to Au–S interactions, suggesting that these effects are rather general.

There has been tremendous interest in using the electronic properties of small organic molecules because they offer the prospect of fabricating ultra-high density electronic circuits as components for molecular computers[1], which will be an important issue for forthcoming nanotechnology (for a review see, for example, ref. 2). Molecular electronics is predicted 'to approach reality' (ref. 3) due to the success of many sophisticated experiments revealing a variety of fascinating aspects of charge transport through organic molecules. Even the possibility of molecular spintronics has been discussed[4].

Much effort has been spent to elucidate the electrical properties of single molecules[5–10], groups of molecules arranged within nanoscaled areas[11,12], and extended molecular layers[13–17]. Charge transport has been investigated by local-probe techniques (such as scanning tunnelling microscopy), break-junction techniques, and by fabricating nanoscaled, as well as microscaled, junctions with an organic layer sandwiched between two metallic electrodes. One of the most fundamental factors determining the flow of charge across the metal–molecule–metal junctions, however, is still not well understood: the role of the contact between the molecule(s) and the outside world represented by the metal leads[18–20]. Although experimental hints can be found for modified energy levels of organic molecules due to their chemical interaction with the metal support[21], the impact of the molecules on the electronic structure of the metal electrodes at the metal–molecule interface has not yet been established. However, from the damping of standing electron waves at Cu(111) step edges induced by a molecule, a lowering of the local density of electronic states in the metal has been proposed[22]. Similarly, a reduced DOS at E_F has been predicted for various metal surfaces (Au, Pd, Rh) with submonolayer coverages of sulphur on the basis of density functional theory (DFT) calculations[23–25], thereby representing one of the typical chemical bonds used to attach a variety of different molecules to the corresponding metal electrodes.

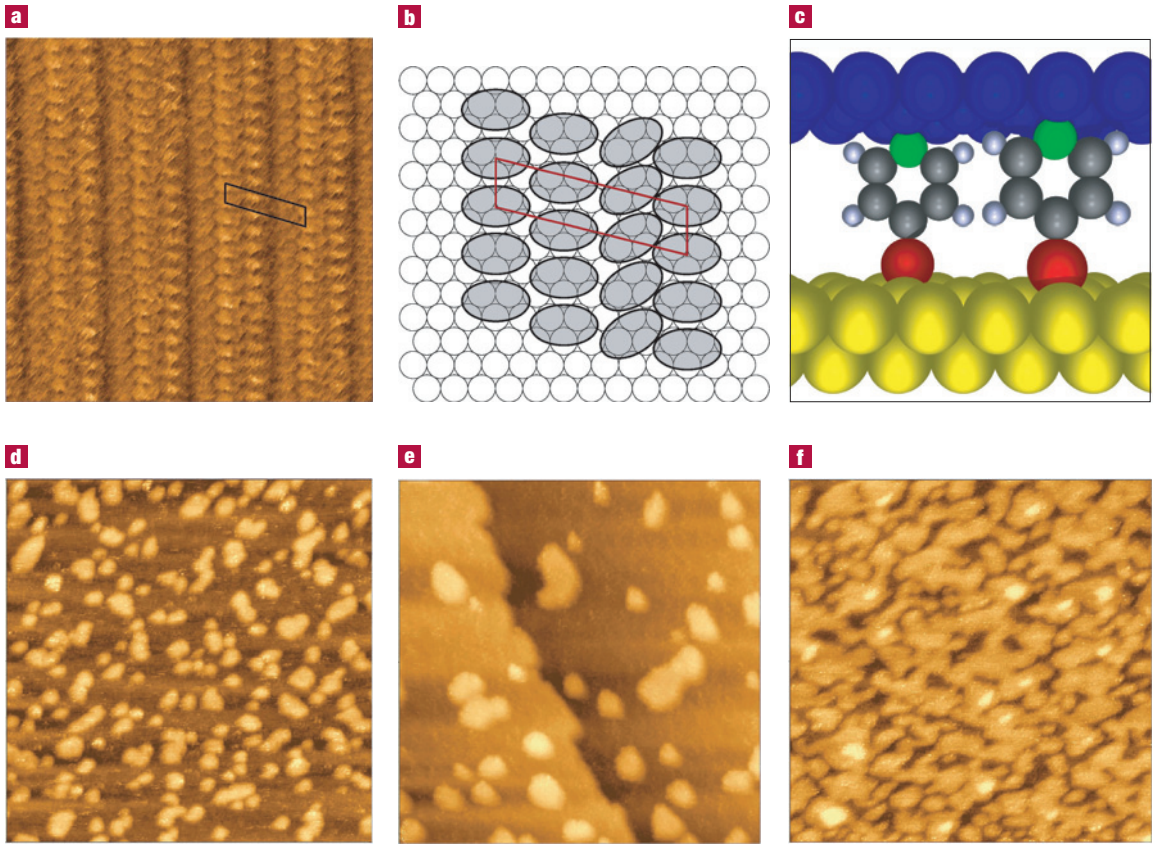

Figure 1 Morphology of the metal–molecule–metal junction after different steps of preparation. Scanning tunnelling microscopy images were taken from the SAM on top of the Au single crystal **a**, before (scan range 10 nm × 10 nm) and (**d–f**), after the deposition of Pd islands using an electrochemical approach: **d**, island size 4.9 nm, scan range 100 nm × 100 nm; **e**, island size 9.0 nm, scan range 103 nm × 103 nm; **f**, 0.7 ML, scan range 100 nm × 100 nm. **b**, The ordered array of molecules visible in **a** is modelled. Here, the open circles represent the Au atoms at the surface of the Au(111) single crystal. The molecules are illustrated as ellipsoids (grey) each centred on top of three Au atoms forming a hollow site containing the S atom of the molecule. The rhomboid (red) describes the unit cell of the ordered array of molecules. **c**, A schematic diagram of the Pd islands on top of the SAM assuming 3 Pd atoms bound to each N atom (Au: yellow; S: red; C: dark grey; H: light grey; N: green; Pd: blue). This way, the topmost Au layer, with a (111)-orientation and the hexagonally close-packed Pd islands also resulting in a (111)-orientation, were expected to show an epitaxial relationship promoted by the organic molecules.

Here, we present experimental evidence for a significantly reduced DOS at E_F, for both metals in a metal–self-assembled monolayer–metal junction, resulting from strong chemical interactions between the molecular layer and its bottom electrode (Au single crystal), as well as its top electrode (Pd islands of monoatomic height). The latter electrode was prepared either as nanometre-sized islands (4.9 nm, 9.0 nm) or as a nearly closed monolayer (0.7 ML), which enabled us to explore the (size dependent) electronic properties of a metal lead during the early stage of contact formation.

All of the samples were prepared by an electrochemical approach[26–28], which combined elements of currentless and electrodeposition. Briefly, a 4MP-SAM was deposited on top of a Au(111) single crystal, forming extraordinary large domains of ordered structures[29] (Fig. 1a) with lattice constants $a = 0.47 \pm 0.05$ nm, $b = 2.2 \pm 0.3$ nm, and $\gamma = 75 \pm 3°$, which is in good agreement with the values reported earlier[29]. Interpreting each characteristic structure as a 4MP molecule, a model for the molecular packing on top of the Au surface is proposed in Fig. 1b ($a = 0.50$ nm, $b = 2.07$ nm, $\gamma = 77°$) assuming a threefold coordination with Au atoms around each S atom. This assumption results in a unit cell with two columns of parallel-oriented molecules, followed by a column of rotated molecules in accordance with the experimental results. In a second step, the complexation between the Pd^{2+} ions and the ring nitrogen of the 4MP molecules was achieved by immersing the SAM-covered gold electrode into a solution containing the metal ions. Finally, by a subsequent potential scan in the negative direction, the complexed metal ions were reduced to Pd^0, allowing the Pd atoms to form strictly two-dimensional metal islands of monoatomic height and variable size on top of the SAM[26,28] (see Fig. 1d–f).

The Pd islands are modelled, in Fig. 1c, assuming that the Pd atoms form a hollow site of three-fold symmetry containing the N atom of the molecule. Consequently, the hexagonally close-packed topmost Au layer corresponding to the (111) crystal orientation, and the hexagonally close-packed Pd islands corresponding to the highest density of atoms in a two-dimensional arrangement, are expected to show an epitaxial relationship promoted by the organic molecules (see below). It should be emphasized that, after depositing the Pd islands, the order of the 4MP molecule array disappears, pointing to local stress within the organic layer induced by the interaction between the molecules and the metal islands.

Figure 2a summarizes the ultraviolet photoelectron spectroscopy (UPS) valence-band spectra obtained from the

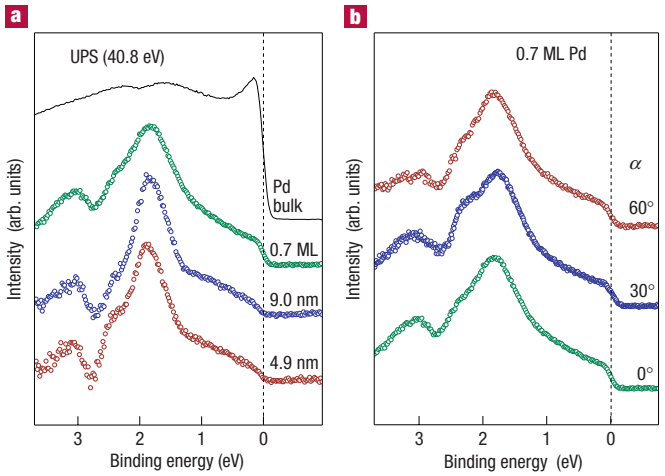

Figure 2 UPS spectra acquired from Pd-covered samples after subtracting the contribution due to the support, thus only representing the properties of the Pd contacts. a, The results measured in the normal direction on different island sizes and the 0.7 ML sample. **b**, Angular-dependent spectra for a 0.7 ML film.

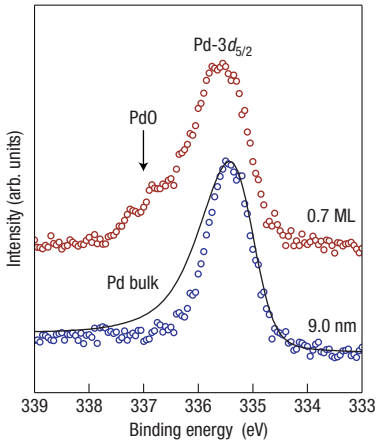

Figure 3 Pd-3$d_{5/2}$ core-level spectra measured with monochromatized X-rays. The solid line represents bulk Pd, whereas the open symbols reveal the results obtained for 9 nm Pd islands (bottom curve) as well as for a 0.7 ML Pd film (top curve).

different samples, after subtracting the contribution arising from the support (measured under identical conditions on the sample shown in Fig. 1a), in comparison to a clean Pd bulk reference sample. Three characteristic features can be recognized at binding energies E_B of 1.8, 2.4 and 3.1 eV, which are common to all three island sizes but which differ significantly from the bulk Pd spectrum. The latter clearly shows a high intensity at the Fermi energy ($E_B = 0$), which is drastically reduced in the nearly closed Pd monolayer, or even absent in the nanometre-sized islands. This indicates a size-induced metal–non-metal transition in the electronic DOS. For oriented layers, however, such a conclusion based on photoemission has to be critically tested, because angular-dependent photoionization cross-sections might prevent the detection of all of the electronic states. To analyse the influence of such effects, angular-dependent measurements were performed on the 0.7 ML film (Fig. 2b). Here, all of the characteristic features in the valence-band structure are found to be independent of the detection angle, proving that it is correct to interpret the UPS spectra in terms of the electronic DOS.

This conclusion is further corroborated by core-level spectroscopy on the Pd-3*d* doublet. Although the Pd-3*d* binding-energy range interferes with the Au-4*d* emission from the support, the Pd contribution can be well separated by subtracting the spectrum acquired from the pure SAM on Au. The result of such a procedure is shown in Fig. 3, where the Pd-3$d_{5/2}$ spectrum measured on 9-nm islands is compared to spectra of a bulk Pd reference sample as well as of the 0.7 ML Pd film, respectively. Identical binding-energy positions are found for all of the samples, providing evidence again for the reduced chemical state (Pd^0) of the Pd atoms deposited on top of the SAM. On the other hand, characteristic differences exist with respect to the line shape. Focusing first on the lower spectra in Fig. 3, a well-pronounced asymmetry towards higher binding energies can be recognized for the bulk sample (solid line), reflecting the creation of electron–hole pairs during the photoemission process in the vicinity of E_F. Such a large asymmetry reflects a high DOS at E_F (ref. 30), confirming the UPS results presented in Fig. 2. In contrast, the line-shape acquired from the 9 nm Pd islands (Fig. 3, bottom curve, circles) is highly symmetric, thereby indicating a vanishing DOS at E_F. Hence, the spectra presented in Fig. 2 can be interpreted in terms of the electronic DOS, thus allowing the comparison to band-structure calculations (see below).

It is worth mentioning that the spectrum for the 0.7 ML film also exhibits an increased intensity visible at higher binding energies. This, however, does not reflect an intrinsic asymmetry of the Pd-3*d* lines. Rather, it indicates the presence of a chemically shifted component, which can easily be identified as PdO. Hence, Pd oxidation starts only in the case of a metallic behaviour of these contacts (non-zero DOS at E_F), whereas non-metallic nanometre-sized islands exhibit an enhanced stability against oxidation.

Self-consistent periodic DFT calculations were carried out as described elsewhere[31] using the Vienna *ab initio* simulation package 'VASP' (ref. 32). Briefly, the exchange–correlation effects were treated within the generalized gradient approximation using the PBE functional[33]. The ionic cores were described using the projected augmented wave (PAW) method[34], and the Kohn–Sham one-electron valence states were expanded in a basis of plane waves with a cutoff energy of 400 eV.

The DFT results obtained for a fully relaxed, non-interacting, densely packed monolayer of Pd atoms are summarized in Fig. 4 (curve (1)). In this case, a nearest-neighbour distance of 0.263 nm is obtained, leading to a DOS that basically consists of three pronounced peaks, a finite DOS at E_F and a bandwidth of 4.7 eV for the occupied electronic states. If compared to the experimental spectrum measured for the 0.7 ML film (curve (5)), the calculated bandwidth of the free monolayer is apparently significantly overestimated. Additionally, the large discrepancies in the peak positions are striking.

Assuming, however, a heteroepitaxial growth of the Pd film with respect to the Au crystal promoted by the SAM, a nearest-neighbour distance of 0.288 nm is expected for the Pd atoms in the ideal case. On the other hand, the missing molecular order between the metal islands after Pd deposition indicating local stress fields, suggests the presence of a reduced lattice parameter. Thus, the DFT calculations were repeated for a free Pd monolayer with a fixed nearest-neighbour distance of 0.280 nm, resulting in a DOS as included in Fig. 4 (curve (2)). Obviously, a much better agreement is achieved between theory and experiment with respect to the bandwidth, as well as for the position of the two

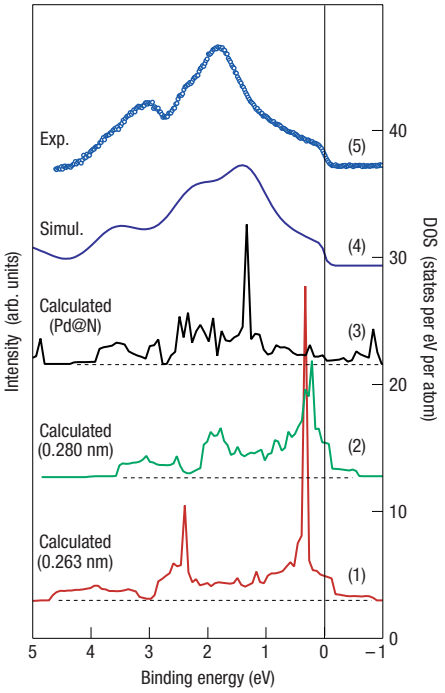

Figure 4 Electronic DOS as calculated within DFT for a Pd monolayer together with experimental results for a 0.7 ML film deposited on top of the SAM. Curve (1) shows the DFT results for a free, relaxed Pd monolayer. Curves (2) and (3) have been calculated on the basis of an expanded lattice parameter (representing heteroepitaxial growth on top of the SAM) without (2) and with (3) chemical interaction with the supporting SAM. Curve (4) is obtained by convolution of (3) with a lorentian reflecting the finite lifetime of the photoionized atoms, followed by convolution with a gaussian representing the experimental energy resolution.

characteristic features found at higher binding energies. However, theory still expects a high DOS peak close to the Fermi level, which is definitely not present in the experimental data. This discrepancy can be better understood by analysing the symmetry of the single-particle wavefunctions related to this peak. Here, we find $4d_{Z^2}$ orbitals extending to a high degree in the normal direction, thus representing those electronic states that most probably interact with the underlying molecules.

Consequently, the DFT calculations were modified to include Pd interactions with the ring nitrogen according to the model shown in Fig. 1c. This modification finally leads to a DOS distribution (Fig. 4, curve (3)), which, after taking into account the finite energy resolution of the experimental setup as well as the generally observed broadening of the spectroscopic features due to the finite lifetime of the photoionized states (Fig. 4, curve (4)), agrees reasonably well with the experimental results. Hence, clear indications are obtained for chemical interactions between the 4MP molecules and the Pd monolayer, leading to a shift towards higher binding energies of the involved states by more than 1 eV. This, by itself, results in a significant reduction of the DOS at E_F by a factor of 4 (compare curves (2) and (3)) having consequences for any charge transport across the metal–molecule interface. The agreement between the simulated and the experimental spectrum might even be improved by taking into account not only the ring nitrogen but the complete organic molecule including its Au support. This, however, is beyond the scope of the present work, but will be investigated in more detail in future studies.

There is still another important point to note. Similar chemical interactions with the SAM are also expected for the nanometre-sized Pd islands, which should consequently reveal a reduced, but non-zero, DOS at E_F. This clearly contrasts with the spectroscopic findings of a non-metallic behaviour in the size range below 10 nm, suggesting the importance of additional effects, such as size-dependent interactions with the underlying SAM or bonding, to the nitrogen, of molecules close to the perimeter of the Pd islands. Unfortunately, a full *ab initio* treatment of such systems is not possible yet owing to the huge number of atoms involved.

Turning now to the second interface in the metal–SAM–metal junction, that is, to the contact area between the SAM and its Au support, we find 21.4% of the Au surface covered with sulphur atoms according to the structural model presented in Fig. 1b,c. Assuming that the Au–S bonds are dominating the interface properties, DFT results from the literature can be used to estimate the influence of the organic molecules on the electronic properties of the support. In this case, for 25% of a Au(111) surface covered with sulphur atoms, a significantly reduced DOS at E_F is predicted for a 4-ML slab of Au (ref. 23), resulting in a calculated reduction to 56% of the bulk value for the topmost Au layer (J. A. Rodriguez, private communication).

To unravel the electronic structure of the topmost Au layer, which is in direct contact with the SAM, angle-resolved UPS measurements were carried out on the sample shown in Fig. 1a. The corresponding results are summarized in Fig. 5 where, in part a, the valence-band structures of the reference systems, that is, the pure molecules deposited as a thin layer on top of a Si wafer, and a clean Au single crystal are shown. When comparing the valence-band shape of both reference samples, the insulating behaviour of the molecules becomes obvious with a HOMO–LUMO gap of at least 4 eV. Consequently, within a binding-energy range of 0–4 eV, photoelectrons emitted from the Au–SAM sample can safely be assigned to originate only from the Au support. This, on the other hand, allows us to interpret angle-resolved spectra within this binding-energy range (Fig. 5b) as representation of the surface region of the Au support. As can be seen in Fig. 5, a decrease in the DOS at E_F is observed for increasing detection angles (corresponding to an increasing surface sensitivity). Taking into account the thermally induced broadening of the Fermi edge according to the Fermi function, as well as the finite energy resolution of the electron energy analyser, the decrease in intensity at E_F as a function of the detection angle can be estimated as shown in Fig. 5c (squares). Assuming that the topmost atomic layer is affected most by the contact to the SAM, and approximating that the second layer has nearly bulk properties, the measured intensity at E_F can be interpreted as (angle-dependent) superposition of the intensity arising from bulk-like (buried) Au, and the intensity emitted from the modified top layer. Taking into account a mean free path value of 0.68 nm (ref. 35) for photoelectrons emitted from the Fermi edge, and fitting the experimental data with a standard formula[36] for angle-resolved photoemission (Fig. 5c, solid line), a decrease to 46% of the value of bulk Au is derived, which agrees reasonably well with the expectations based on the DFT calculations as mentioned previously.

Thus, modifications of the electronic structure of the metal electrode are also found at the Au–S interface, suggesting that such modifications of the metallic contacts, induced by strong chemical bonds to organic molecules, are a general phenomenon. Comparing the reduction of the DOS at E_F for both metals, a decrease by a factor of about 2 is found at the Au–S interface, whereas according to our DFT calculations at the Pd–N interface, a factor of 4 is expected. Experimentally, for Pd, the interaction between the molecules and the metal overlayer even results in non-metallic behaviour (vanishing DOS at E_F) if the diameter of

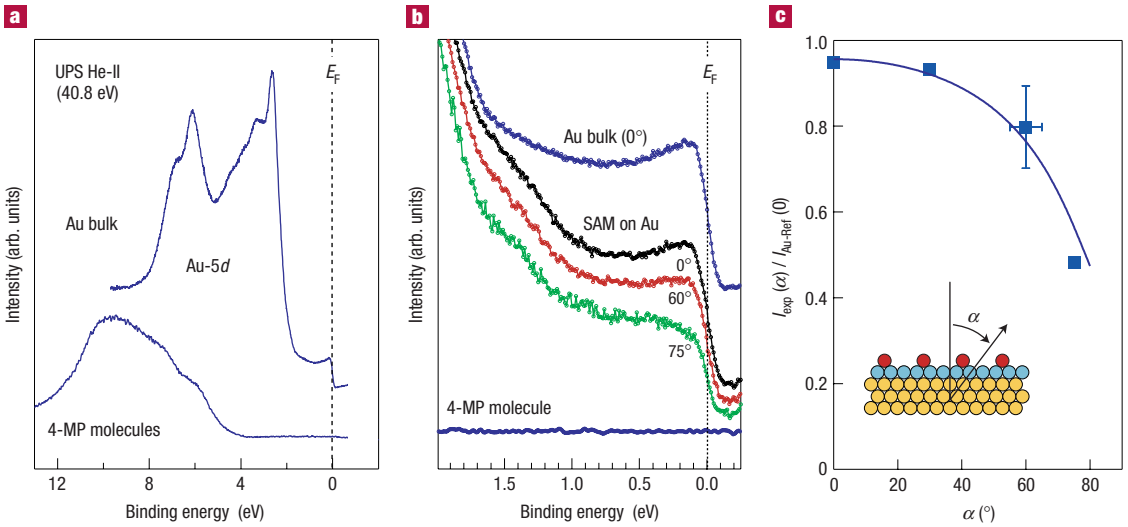

Figure 5 Photoemission results ($h\nu = 40.8$ eV) related to the Au–SAM interface. a, Shows the valence-band structure of the organic molecules deposited as a thin layer on a silicon wafer, together with a spectrum measured on a clean Au single crystal both serving as reference systems. The top spectrum has been measured on a Au bulk sample, the bottom spectrum on a thin film of 4-MP molecules. **b**, Enlarged view of the binding-energy range close to E_F showing a decreasing intensity at E_F for increasing detection angles (increasing surface sensitivity). **c**, The corresponding intensity values (full squares) for increasing detection angles normalized to the intensity of the Au reference measured under normal incidence. Using these data and assuming a two-layer model, a DOS decrease by more than a factor of 2 can be extracted for the topmost Au layer as compared with bulk Au. The horizontal error bar indicates the (maximum) uncertainty in detection angle induced by a possible misalignment of the sample surface with respect to the manipulator system of the electron spectrometer. The vertical error bar reflects the standard deviation of the corresponding intensities at E_F obtained by a fitting procedure while taking into account the thermally induced broadening of the Fermi function and the finite energy resolution of the electron energy analyser.

the metal electrode is reduced to a value of the order of 10 nm. Nanometre-sized metal probes, on the other hand, have been used in experiments[37] to characterize the transport properties of groups of molecules. Based on the present results, a principal problem with such measurements has to be considered: due to interactions with the molecules, a metallic nanocontact can turn non-metallic, as observed above for the Pd islands. The consequence on electron transport at low bias voltages immediately becomes clear by considering[37–44] tunnelling processes between the two metal electrodes through the organic molecules with a HOMO–LUMO gap. Close to zero bias, the (small) conductance G of such a metal–molecule–metal junction can be expressed[42,44,45] as $G(E_F) = G_0(E_F)e^{-\gamma L}$ with G_0 representing the so-called contact conductance, γ the tunnel junction inverse decay length which is a function of the HOMO–LUMO gap of the molecule(s) as well as the effective mass of the tunnelling electrons, and L the distance between the leads. The properties of the metal electrodes are taken into account[42,44] by means of the contact conductance $G_0(E_F)$ which, to first-order approximation (that is, according to the Fermi golden rule) should be proportional to the electronic DOS at the Fermi level at the surface of the two metal pads. Thus, any distinct reduction of the DOS at E_F of the two electrodes will result in a reduced contact conductance, which, in the case of the small Pd islands with non-metallic properties, might even add another large tunnelling resistance to the total resistance of the junction.

For higher voltages applied to the junction, the effect of a reduced DOS at E_F for both electrodes may be even stronger. In that case, energy levels assigned to molecular orbitals can be adjusted to match continuum states in the electrode materials, resulting in high transmission coefficients (of the order of 1) for charge transport through the molecules. In this situation, a drastically increased contact resistance, as compared with the undisturbed electrode material, might even dominate the transport properties of the whole junction. Of course, this rather qualitative picture requires a full theoretical treatment to understand all of the consequences on the transport properties, which is beyond the scope of this article. On the other hand, the observation of vanishing metallic properties of nano-sized electrodes attached to a group of organic molecules might open a new perspective of realizing single electron tunnelling through an 'organic quantum dot', which could lead to the design of organic single-electron transistors as attractive components of future molecular electronics devices.

These results are expected to have a strong impact on future studies trying to establish and control all of the factors relevant for electrical transport in nanoscaled organic systems, a necessary requirement for the development of molecular electronics.

METHODS

The chemical state of the samples was analysed by X-ray photoelectron spectroscopy (XPS) using monochromatized X-rays (1,486.6 eV) as provided by a commercial photoemission system (Fisons ESCALAB 210). The electronic structure of the Pd islands was determined using UPS carried out with non-polarized He-II radiation (40.8 eV) from a gas discharge lamp and setting the angular acceptance of the energy analyser to its maximum value (±12°). Radiation damage to the SAM, as induced by secondary electrons[46], was avoided by reducing the photon flux of both sources, and by the small spot size (<1 mm) of the two photon beams (XPS, UPS), allowing a certain sample position to be probed for times less than 1 h, followed by moving to a new position. During these probing times, no measurable decrease of the corresponding core-level or valence-band intensities, or changes in their line shapes, were detected.

It is worth mentioning that, for the current metal–molecule–metal junction, photoemission experiments carried out with synchrotron radiation at an undulator beamline immediately resulted in the destruction of the molecular device as shown by vanishing Pd-3*d* core-level intensities.

Received 2 September 2005; accepted 23 January 2006; published 2 April 2006.

References

1. Seminario, J. M. & Tour, J. M. Ab initio methods for the study of molecular systems for nanometre technology: Toward the first-principles design of molecular computers. *Ann. NY Acad. Sci.* **852,** 68–94 (1998).
2. Joachim, C., Gimzewski, J. K. & Aviram, A. Electronics using hybrid-molecular and mono-molecular devices. *Nature* **408,** 541–548 (2000).
3. Seminario, J. M. Molecular electronics—approaching reality. *Nature Mater.* **4,** 111–113 (2005).
4. Rocha, A. R. *et al.* Towards molecular spintronics. *Nature Mater.* **4,** 335–339 (2005).
5. Reed, M. A., Zhou, C., Muller, C. J., Burgin, T. P. & Tour, J. M. Conductance of a molecular junction. *Science* **278,** 252–254 (1997).
6. Fink, H.-W. & Schönenberger, C. Electrical conduction through DNA molecules. *Nature* **398,** 407–410 (1999).
7. Porath, D., Bezryadin, A., Vries, S. D. & Dekker, C. Direct measurement of electrical transport through DNA molecules. *Nature* **403,** 635–638 (2000).
8. Cui, X. D. *et al.* Reproducible measurements of single-molecule conductivity. *Science* **294,** 571–574 (2001).
9. Reichert, J. *et al.* Driving current through single organic molecules. *Phys. Rev. Lett.* **88,** 176804 (2002).
10. Gittins, D. I., Bethell, D., Schiffrin, D. J. & Nichols, R. J. A nanometre-scale electronic switch consisting of a metal cluster and redox-addressable groups. *Nature* **408,** 67–69 (2000).
11. Chen, J., Reed, M. A., Rawlett, A. M. & Tour, J. M. Large on-off ratios and negative differential resistance in a molecular electronic device. *Science* **286,** 1550–1552 (1999).
12. Blum, A. S. *et al.* Molecularly inherent voltage-controlled conductance switching. *Nature Mater.* **4,** 167–172 (2005).
13. Vilan, A., Shanzer, A. & Cahen, D. Molecular control over Au/GaAs diodes. *Nature* **404,** 166–168 (2000).
14. Haag, R., Rampi, M. A., Holmlin, R. E. & Whitesides, G. M. Electrical breakdown of aliphatic SAMs used a nanometer-thick organic dielectrics. *J. Am. Chem. Soc.* **121,** 7895–7906 (1999).
15. Collier, C. P. *et al.* Electronically configurable molecular-based logic gates. *Science* **285,** 391–394 (1999).
16. Collier, C. P. *et al.* A (2)catenane-based solid state electronically reconfigurable switch. *Science* **289,** 1172–1175 (2000).
17. Kagan, C. R. *et al.* Evaluations and considerations for self-assembles monolayer field-effect transistors. *Nano Lett.* **3,** 119–124 (2003).
18. Hipps, K. W. It's all about contacts. *Science* **294,** 536–537 (2001).
19. Kushmerick, J. G. Metal-molecule contacts. *Mater. Today* 26–30 (July/August, 2005).
20. Cahen, D., Kahn, A. & Umbach, E. Energetics of molecular interfaces. *Mater. Today* 32–41 (July/August, 2005).
21. Silien, C., Pradhan, N. A., Ho, W. & Thiry, P. A. Influence of adsorbate-substrate interaction on the local electronic structure of C60 studied by low-temperature STM. *Phys. Rev. B* **69,** 115434 (2004).
22. Moresco, F. *et al.* Probing the different stages in contacting a single molecular wire. *Phys. Rev. Lett.* **91,** 036601 (2003).
23. Rodriguez, J. A. *et al.* Coverage effects and the nature of the metal-sulfur bond in S/Au(111): high-resolution photoemission and density-functional studies. *J. Am. Chem. Soc.* **125,** 276–285 (2003).
24. Wei, C. M., Gross, A. & Scheffler, M. Ab initio calculation of the potential energy surface for the dissociation of H2 on the sulfur-covered Pd(100) surface. *Phys. Rev. B* **57,** 15572–15584 (1998).
25. Feibelman, P. J. & Hamann, D. R. Electronic structure of a "poisoned" transition-metal surface. *Phys. Rev. Lett.* **52,** 61–64 (1984).
26. Baunach, T. *et al.* A new approach to the electrochemical metallization of organic monolayers: Pd deposition onto a 4, 4′-dithiodipyridine-SAM. *Adv. Mater.* **16,** 2024–2028 (2004).
27. Ivanova, V., Baunach, T. & Kolb, D. M. Metal deposition onto a thiol-covered gold surface: A new approach. *Electrochim. Acta* **50,** 4283–4288 (2005).
28. Manolova, M. *et al.* Metal deposition onto thiol-covered gold: Pt on a 4-mercaptopyridine SAM. *Surf. Sci.* **590,** 146–153 (2005).
29. Zhou, W., Baunach, T., Ivanova, V. & Kolb, D. M. Structure and electrochemistry of 4, 4′-dithiodipyridine self-assembled monolayers in comparison with 4-mercaptopyridine self-assembled monolayers on Au(111). *Langmuir* **20,** 4590–4595 (2004).
30. Wertheim, G. K. & Citrin, P. H. Photoemission in solids I. *Topics Appl. Phys.* **26,** 197–236 (1978).
31. Roudgar, A. & Groß, A. Local reactivity of supported metal clusters: Pd_n on Au(111). *Surf. Sci.* **559,** L180–L186 (2004).
32. Kresse, G. & Furthmüller, J. Efficient iterative schemes for ab initio total-energy calculations using a plane-wave basis set. *Phys. Rev. B* **54,** 11169–11186 (1996).
33. Perdew, J. P., Burke, K. & Ernzerhof, M. Generalized gradient approximation made simple. *Phys. Rev. Lett.* **77,** 3865–3868 (1996).
34. Kresse, G. & Joubert, D. From ultrasoft pseudopotentials to the projector augmented-wave method. *Phys. Rev. B* **59,** 1758–1775 (1999).
35. Penn, D. R. Electron mean-free-path calculations using a model dielectric function. *Phys. Rev. B* **35,** 482–486 (1981).
36. Lin, T.-S. *et al.* Characterization of the alpha-Sn/CdTe(110) interface by angle-resolved X-ray photoemission. *Surf. Sci.* **183,** 113–122 (1987).
37. Wang, W., Lee, T. & Reed, M. A. Electron tunneling in self-assembled monolayers. *Rep. Prog. Phys.* **68,** 523–544 (2005).
38. Samanta, M. P., Tian, W., Datta, S., Henderson, J. I. & Kubiak, C. P. Electronic conduction through organic molecules. *Phys. Rev. B* **53,** R7626–R7629 (1996).
39. Datta, S. *et al.* Current-voltage characteristics of self-assembled monolayers by scanning tunneling microscopy. *Phys. Rev. Lett.* **79,** 2530–2533 (1997).
40. Derosa, P. A. & Seminario, J. M. Electron transport through single molecules: scattering treatment using density functional and green function theories. *J. Phys. Chem. B* **105,** 471–481 (2001).
41. Xue, Y. & Ratner, M. A. Microscopic study of electrical transport through individual molecules with metallic contacts. I. Band lineup, voltage drop, and high-field transport. *Phys. Rev. B* **68,** 115406 (2003).
42. Lahmidi, A. & Joachim, C. Decay of the molecular wire conductance with length: the role of spectral rigidity. *Chem. Phys. Lett.* **381,** 335–339 (2003).
43. Hou, S. *et al.* First-principle calculation of the conductance of a single 4,4 bipyridine molecule. *Nanotechnology* **16,** 239–244 (2005).
44. Stojkovic, S., Joachim, C., Grill, L. & Moresco, F. The contact conductance on a molecular wire. *Chem. Phys. Lett.* **408,** 134–138 (2005).
45. Magoga, M. & Joachim, C. Conductance and transparence of long molecular wires. *Phys. Rev. B* **56,** 4722–4729 (1997).
46. Jäger, B. *et al.* X-ray and low energy electron induced damage in alkanethiolate monolayers on Au-substrates. *Z. Phys. Chem.* **202,** 263–272 (1997).

Acknowledgements

We thank J. A. Rodriguez (Chemistry Department, Brookhaven National Laboratory) for helpful discussions and M. Manolova (Abteilung Elektrochemie, Universität Ulm) for technical assistance. This work was supported by the Deutsche Forschungsgemeinschaft (DFG) within SFB 569, the Fonds der Chemischen Industrie, the Swiss National Science Foundation (NF) and the NCCR 'Nanoscale Science'.

Correspondence and requests for materials should be addressed to H.-G.B.

Competing financial interests

The authors declare that they have no competing financial interests.